

Title

Unfolded protein-independent IRE1 activation contributes to multifaceted developmental processes in Arabidopsis

Kei-ichiro Mishiba*, Yuji Iwata, Tomofumi Mochizuki, Atsushi Matsumura, Nanami Nishioka, Rikako Hirata and Nozomu Koizumi

Graduate School of Life and Environmental Sciences, Osaka Prefecture University, 1-1 Gakuencho, Nakaku, Sakai, Osaka, 599-8531, Japan

* Corresponding author:

Kei-ichiro Mishiba

Graduate School of Life and Environmental Sciences, Osaka Prefecture University, 1-1 Gakuencho, Nakaku, Sakai, 599-8531, Japan

e-mail: mishiba@plant.osakafu-u.ac.jp

Abstract

As an initial step for the unfolded protein response (UPR) pathway, the luminal domain of inositol requiring enzyme 1 (IRE1) senses unfolded proteins in the endoplasmic reticulum (ER). Recent findings in yeast and metazoans suggest alternative IRE1 activation without the sensor domain, although its mechanism and physiological significance remain to be elucidated. In Arabidopsis, the *IRE1A* and *IRE1B* double mutant (*ire1a/b*) is unable to activate cytoplasmic splicing of *bZIP60* mRNA and regulated IRE1-dependent decay (RIDD) under ER stress, while the mutant does not exhibit severe developmental defects and is fertile under non-stress conditions. In this study, we focused on a third Arabidopsis *IRE1* gene, designated as *IRE1C*, whose product lacks a sensor domain. We found that even though *ire1c* and *ire1a/c* mutants did not exhibit defective *bZIP60* splicing and RIDD under ER stress, the *ire1a/b/c* triple mutant is lethal. Heterozygous *IRE1C* (*ire1c/+*) mutation in the *ire1a/b* mutants resulted in growth defects and reduction of the number of pollen grains. Genetic analysis revealed that *IRE1C* is required for male gametophyte development in the *ire1a/b* mutant background. Expression of a mutant form of IRE1B that lacks the luminal sensor domain (Δ LD) in the *ire1a/b* mutant did not complement defects in ER stress-dependent *bZIP60* splicing and RIDD. Nevertheless, expression of Δ LD complemented a developmental defect in the male gametophyte in *ire1a/b/c* haplotype. *In vivo*, the Δ LD protein was activated by glycerol treatment that increases the composition of saturated lipid and was able to activate RIDD but not *bZIP60* splicing. Phenotypes of *IRE1B* mutants lacking the sensor domain produced by CRISPR/Cas9-mediated gene editing in the *ire1a/c* mutant background were essentially same as those of Δ LD-expressing *ire1a/b* mutant. These observations suggest that IRE1 contributes to plant development, especially male gametogenesis, using an alternative activation mechanism that bypasses the unfolded protein-sensing luminal domain.

Introduction

The endoplasmic reticulum (ER) in eukaryotes copes with an accumulation of unfolded proteins by activating the unfolded protein response (UPR), which increases protein folding capacity and attenuates protein synthesis in the ER (Walter & Ron, 2011). Inositol-requiring enzyme 1 (IRE1) is the primary transducer of the UPR. IRE1 consists of an N-terminal sensor domain facing the ER lumen, a single transmembrane helix (TMH) embedded in the ER membrane, and kinase and ribonuclease (RNase) domains at its C-terminus on the cytosolic side (Nikawa & Yamashita, 1992; Sidrauski & Walter, 1997). Under ER stress, IRE1 senses unfolded proteins in the ER, which causes autophosphorylation of IRE1 to exert RNase activity for cytoplasmic splicing. Targets of the cytoplasmic splicing are mRNAs encoding UPR-specific transcription factors, such as HAC1 in yeasts (Sidrauski & Walter, 1997), XBP1 in metazoans (Yoshida *et al.*, 2001) and bZIP60 in Arabidopsis (Deng *et al.*, 2011; Nagashima *et al.*, 2011). Activated IRE1 also degrades mRNAs encoding secretory

pathway proteins, designated as the Regulated IRE1-Dependent Decay (RIDD) of mRNAs in fission yeast (Kimmig *et al*, 2012), metazoans (Hollien & Weissman, 2006; Iqbal *et al*, 2008; Han *et al*, 2009; Hollien *et al*, 2009) and plants (Mishiba *et al*, 2013; Hayashi *et al*, 2016). Although distinct catalytic mechanisms between cytoplasmic splicing and RIDD has been reported (Tam *et al*, 2014), how IRE1 outputs these two modules during physiological and developmental processes is still unclear (Maurel *et al*, 2014).

Even though IRE1-deficient mice (Zhang *et al*, 2005) and flies (Ryoo *et al*, 2013) cause embryonic lethality, IRE1-deficient yeast (Nikawa & Yamashita, 1992; Kimmig *et al*, 2012) and worms (Shen *et al*, 2001) are viable. In plants, Arabidopsis IRE1A- and IRE1B-defective mutants do not exhibit severe developmental phenotypes under normal conditions (Nagashima *et al*, 2011; Chen & Brandizzi, 2011), whereas rice homozygotes that express kinase-defective IRE1 is lethal (Wakasa *et al*, 2012; note that rice has one *IRE1* gene). This different consequence of IRE1 mutation in phenotypes between Arabidopsis and rice prompted us to investigate the degree of contribution that IRE1 makes to plant development.

In recent years, activation of IRE1 caused by lipid perturbation was observed in yeast (Promlek *et al*, 2011) and mouse cells (Volmer *et al*, 2013). This IRE1 activation does not require sensing of unfolded proteins by the luminal domain of IRE1, but does require an amphipathic helix (AH) adjacent to the transmembrane helix (TMH) to sense ER membrane aberrancies (Halbleib *et al*, 2017). Although physiological functions of lipid-dependent IRE1 activation is less well known, it has been presumed that the unfolded protein-independent mechanism allow cells to prospectively adopt their ER folding capacity (Volmer & Ron, 2015). For instance, mutant worms with decreased membrane phospholipid desaturation activate IRE1 without promoting unfolded protein aggregates (Hou *et al*, 2014). However, there are no studies directly addressing the importance of the unfolded protein-independent IRE1 activation in developmental processes in multicellular organisms.

In this report, we investigated the contribution of IRE1 lacking its sensor domain to Arabidopsis development. We found that a third Arabidopsis *IRE1* gene, encoding sensor domain-lacking IRE1, is functional and that the triple mutant of the three *IRE1* (*IRE1A-C*) genes is lethal. Our analyses with plants that express mutant IRE1B proteins without the sensor domain suggest contribution of unfolded protein-independent IRE1 activation to multifaceted developmental processes in Arabidopsis.

Results

Loss of function of IRE1C does not alter ER stress response

In addition to the *IRE1A* and *IRE1B* genes, Arabidopsis contains an *IRE1-like* gene (AT3G11870; designated as *IRE1C* hereafter), whose product lacks a sensor domain (Fig. 1A). The sensor domain-lacking IRE1 was also found in some other Brassicaceae species, such as *Camelina sativa*,

and phylogenetic analysis showed that the IRE1C forms an independent cluster from IRE1A and IRE1B groups in dicotyledonous plants (Fig. 1B). A T-DNA insertion mutant of *ire1c* (SALK_204405; Fig. S1A) and *ire1a ire1c* (designated as *ire1a/c* hereafter) double mutants did not exhibit any visible phenotypic alterations in normal growth conditions (Fig. 1C). Consistent with the previous studies (Nagashima *et al*, 2011; Mishiba *et al*, 2013), susceptibility to ER stress inducer, dithiothreitol (DTT) was more apparent in *ire1a/b* mutant than those in WT, *ire1a*, and *ire1b* mutants (Fig. 1D). The susceptibility to DTT in *ire1c* and *ire1a/c* mutants was same as that in WT (Fig. 1D). To detect bZIP60 splicing and RIDD in the IRE1 mutants under ER stress, expressions of *BiP3* and *PR-4* mRNA, which are the typical targets of bZIP60 (Iwata & Koizumi, 2005) and RIDD (Mishiba *et al*, 2013), respectively, were analyzed by northern blotting. Up-regulation of *BiP3* mRNA and down-regulation of *PR-4* mRNA by tunicamycin (Tm) treatment was observed in *ire1c* and *ire1a/c* mutants as well as WT, *ire1a*, and *ire1b* mutants, but not in *ire1a/b* mutant (Fig. 1E). These results indicate that IRE1C, which lacks a sensor domain, does not contribute to ER stress response in Arabidopsis.

A triple mutant of IRE1A, IRE1B, and IRE1C is lethal

We tried to produce *ire1a/b/c* triple mutant by crossing *ire1a/b* with *ire1c* mutants. We obtained three F₂ plants heterozygous for *ire1c* (designated as *ire1c/+*) and homozygous for *ire1a* and *ire1b*. Genotyping of their self-pollinated progenies showed that no plants homozygous for *ire1c* were obtained among 108 plants analyzed (Table 1, Fig. S1B). Additionally, unexpected segregation of homozygotes and heterozygotes for IRE1C (+/+ : *ire1c/+* = 1.0:0.3) was observed. These results indicate that *ire1a/b/c* triple mutant is lethal. The *ire1a/b ire1c/+* plants exhibited growth retardation (Fig. 2A) and reduced seed set (Figs. 2B, 2C) compared to the *ire1a/b +/+* siblings. Pollen development was especially impaired in the *ire1a/b ire1c/+* plants, whereas *ire1c* and *ire1a/c* mutants did not affect pollen development and seed set (Fig. 2C). No transmission of the *ire1c* allele through male gametophyte were shown after reciprocal crossing between *ire1a/b* and *ire1a/b ire1c/+* mutants (Table 1). Transgenic plants carrying IRE1C promoter-driven *GUS* reporter gene construct (Fig. S2A) showed that IRE1C is expressed in anther (Fig. S3A) and embryo (Fig. S3B). No visible GUS staining was observed in vegetative tissues (root, leaf, and stem) of young seedlings with or without stress treatments (Fig. S3C). These observations are qualitatively consistent with the microarray database (Arabidopsis eFP browser; <http://bar.utoronto.ca/efp/cgi-bin/efpWeb.cgi>), which shows that the IRE1C gene is scarcely expressed in vegetative tissues. Taken together, IRE1C, which lacks a sensor domain, contributes to male gametophyte development and acts redundantly with IRE1A and IRE1B.

Mutant IRE1B lacking the sensor domain is not responsible for UPR signal transduction

Because *ire1a/c* mutants retain fertility and IRE1-dependent UPR signal transduction, IRE1B possibly plays a role in both UPR and developmental processes. To investigate an unknown IRE1 function, we generated a construct expressing FLAG-tagged wild-type (WT) form of IRE1B as well as those with

kinase (K487A), RNase (K821A), and luminal sensor-deletion (Δ LD) mutants under the control of its native promoter (Figs. 3A, S2B). For comparison, we generated constructs expressing FLAG-tagged wild-type (WT) IRE1A as well as mutant IRE1A with kinase (K442A) and RNase (K781A) mutation under the IRE1A native promoter (Figs. 3A, S2B). These constructs were introduced into the *ire1a/b* mutant using *Agrobacterium*-mediated transformation and T₃ homozygous transgenic plants were used for further analyses. All of the WT and mutant IRE1 constructs expressed expected sizes of IRE1 proteins in seedlings (Fig. 3B). Up- and down-regulation of *BiP3* and *PR-4* mRNA, respectively, by Tm treatment were restored in the FLAG-IRE1A(WT) and FLAG-IRE1B(WT) transgenic plants, but not in kinase-, RNase-, and Δ LD-expressing transgenic plants (Fig. 3C). We next analyzed *in vivo* phosphorylation of FLAG-IRE1B under ER stress by Phos-tag-based western blot (Yang et al, 2010). A slower migrating, phosphorylated form of IRE1B was detected in Tm- and DTT-treated FLAG-IRE1B(WT) plants but not in the DTT-treated K487A plants (Fig. 3D). Consistent with the results of *BiP3* and *PR-4* expressions, expression of FLAG-IRE1B(WT) restored hypersensitivity of the *ire1a/b* mutant to DTT to the level observed in WT, but expression of Δ LD did not (Fig. 3E). These results indicate that the mutant IRE1B lacking the sensor domain does not contribute to the ER stress response.

FLAG-IRE1B(WT) and Δ LD restore the developmental defects in *ire1a/b ire1c/+* mutant

We crossed the *ire1a/b* mutant plants expressing FLAG-IRE1B(WT) or Δ LD with *ire1a/b ire1c/+* mutant plants. F₁ plants heterozygous for *IRE1C* (*ire1a/b ire1c/+*) were selected and self-pollinated. Among F₂ plants, plants that are homozygous for the transgenes and heterozygous for *IRE1C* were selected for further analyses. Growth defects (Figs. 4A-F) and the reduction of seed set (Figs. 4G-I) in the *ire1a/b ire1c/+* mutant were restored by expression of FLAG-IRE1B(WT) and Δ LD plants. Abortion of pollen development in *ire1a/b ire1c/+* mutant was restored, as well (Figs. 4J-L). At the completion of meiosis, the *ire1a/b ire1c/+* mutant plants expressing FLAG-IRE1B(WT) or Δ LD produced four viable microspores in each tetrad (Figs. 4M, N), whereas the *ire1a/b ire1c/+* mutant frequently produced abnormal tetrads (Fig. 4O).

Impaired pollen development in *ire1a/b/c* gametophyte is restored by Δ LD

Unexpectedly, self-pollinated progenies of the *ire1a/b ire1c/+* plants expressing FLAG-IRE1B(WT) or Δ LD plants segregated with the *IRE1C* allele in ratios of 1.0:1.9:0 (+/+ : c/+ : c/c; n = 154) and 1.0:1.4:0 (n = 237), respectively (Table 2). Nevertheless, their occurrence ratios of the heterozygous allele were higher than that in the *ire1a/b ire1c/+* mutant (1.0:0.30:0; n = 108; Table 1). To determine whether the impaired transmission of the *ire1c* allele through male gametophyte in *ire1a/b ire1c/+* mutant was restored by FLAG-IRE1B(WT) and Δ LD, we performed reciprocal crosses between the *ire1a/b ire1c/+* plants with homozygous FLAG-IRE1B(WT) or Δ LD transgene and wild-type plants. Consistent with the results of the reciprocal crossing between *ire1a/b* and *ire1a/b ire1c/+* (Table 1),

control reciprocal crossing between wild-type and *ire1a/b ire1c/+* showed no transmission of the *ire1c* allele through male gametophyte (Table 2). In the case of the crossing between the wild-type plants as female parents and the *ire1a/b ire1c/+* plants with FLAG-IRE1B(WT) or Δ LD as male parents, progenies having *ire1c/+* allele were obtained in the ratios of 1.0:0.33 (+/+ : c/+; n = 57) and 1.0:0.57 (n = 94), respectively (Table 2). These results indicate that not only FLAG-IRE1B(WT) but also Δ LD can compensate for impaired male gametogenesis in the *ire1a/b/c* haplotype.

To investigate the defect of male gametogenesis in the *ire1a/b/c* haplotype, we observed cross sections prepared from inflorescences of wild-type, *ire1a/b ire1c/+*, and *ire1a/b ire1c/+* expressing Δ LD at different developmental stages. The anther size and the number of pollen grains were reduced in *ire1a/b ire1c/+* compared to wild-type (Fig. 5). Regarding pollen development, no obvious differences were observed between *ire1a/b ire1c/+* and wild-type at stage 8 and 9 (Fig. 5). However, a part of pollen grains collapsed in *ire1a/b ire1c/+* at stage 11 (Fig. 5; indicated by arrowheads). The collapsing pollen grains were also shown in *ire1a/b ire1c/+* expressing Δ LD, but the frequency was very low (Fig. 5; arrowhead). In *ire1a/b ire1c/+* expressing Δ LD, the anther size was restored to the wild-type level (Fig. 5).

Results of the crossing between *ire1a/b ire1c/+* as female parents and *ire1a/b* (Table 1) or wild-type (Table 2) as male parents suggest incomplete female gametogenesis in the *ire1a/b/c* haplotype. However, FLAG-IRE1B(WT) and Δ LD transgenes did not affect the occurrence ratios of heterogeneous *ire1c/+* allele through the female gametophyte (Table 2).

Different IRE1 activation states by saturated fatty acids in the presence or absence of sensor domain

Growing evidence suggests that yeast and metazoan IRE1 have lipid-dependent activation machinery (Volmer & Ron, 2015). Since exogenous application of glycerol is known to reduce oleic acid (18:1) level in Arabidopsis (Kachroo *et al*, 2004), we applied glycerol treatment to Arabidopsis seedlings to increase saturated fatty acid composition. As expected, levels of palmitic acid (16:0) and stearic acid (18:0) were increased after three days of glycerol treatment in wild-type and *ire1a/b* seedlings (Fig. 6A). Glycerol treatment induced *bZIP60* splicing in wild-type but not in *ire1a/b* seedlings (Fig. 6B). Impaired *bZIP60* splicing in *ire1a/b* was restored by expression of FLAG-IRE1A(WT) and FLAG-IRE1B(WT), but not by that of kinase, RNase, and Δ LD mutants (Figs. 6C, S4A, S4B). Accumulation and phosphorylation of the FLAG-IRE1B(WT) protein was observed in the glycerol-treated seedlings (Fig. 6D). Thus, IRE1's kinase, RNase, and sensor domains are responsible for *bZIP60* splicing under glycerol treatment *in vivo*.

To determine whether glycerol treatment induces RIDD, mRNA levels of three RIDD target genes (*PR-4*, *PRX34*, and *MBL1*; Mishiba *et al*, 2013; Iwata *et al*, 2016) was analyzed in the glycerol-treated wild-type and *ire1a/b* seedlings, which were further treated with cordycepin to prevent transcription. Higher expressions of the three genes were observed in the glycerol-treated wild-type and *ire1a/b*

plants compared to untreated control (Fig. 6E). Decrease in *PR-4*, *PRX34* and *MBL1* mRNA abundance was detected within 5 hours of cordycepin treatment in wild-type but not in *ire1a/b* seedlings. The impaired mRNA degradation in *ire1a/b* was restored by expression of FLAG-IRE1B(WT) and Δ LD, but not by that of RNase (K821A) mutant (Fig. 6F). Consistently, while levels of mRNA encoding cytosolic proteins, cFBPase and UGPase, did not show significant difference among the samples irrespective of glycerol treatment (Fig. S4C), expression of *PR-4*, *PRX34*, *MBL1*, and *PME41* (RIDD target; Mishiba *et al*, 2013) mRNAs was increased ($P < 0.05$) in *ire1a/b* and K821A compared to wild-type, FLAG-IRE1B(WT), and Δ LD plants under glycerol treatment (Fig. S4D). Accumulation of Δ LD proteins was observed under glycerol and DTT treatments (Fig. 6G). Phos-tag western blot of Δ LD protein showed two slower migrating bands than unphosphorylated protein in the untreated-, Tm- and DTT-treated plants, whereas only the slowest migrating band was detected in the glycerol-treated plants (Fig. 6H). These results indicate that glycerol treatment stimulate the mutant IRE1 proteins lacking the sensor domain, causing RIDD.

CRISPR/Cas9-induced deletion corresponding to *IRE1B* sensor region in *ire1a/c* mutant

To gain insight into the contribution of the sensor domain-independent IRE1 activation to the developmental process, we tried to induce deletion in the sensor domain-coding region of the *IRE1B* gene in the *ire1a/c* mutant using CRISPR/Cas9 system. *Agrobacterium* harbouring pKIR1.0 binary vector (Tsutsui & Higashiyama, 2017) containing two gRNAs targeting the 5' and 3' ends of the *IRE1B*'s sensor domain-coding region (Figs. 7A, S2C) was used to transform the *ire1a/c* mutant. We selected T₂ lines showing 3:1 segregation ratio for the presence and absence of RFP fluorescence (see Fig. S2C) in seeds and picked up some seeds with no fluorescence, indicative of no T-DNA insertion for further analyses (Tsutsui & Higashiyama, 2017). When we amplify an *IRE1B*-coding genomic region by PCR, we obtained smaller bands than that would be expected from intact *IRE1B* in some T₂ plants, indicating that deletion is successfully introduced. Therefore, their self-progenies (T₃) were used for further analyses. In lines #2-5 and #9-6, all T₃ plants analyzed showed a single, smaller *IRE1B* fragment, indicating homozygous deletion of *IRE1B* locus (Fig. S5A). Sequence analysis showed deletion of 981 and 1,216 bp regions, each corresponding to part of the sensor domain in #2-5 and #9-6, respectively, and 1 bp deletion at the gRNA2 target site was also detected in #2-5 (Fig. 7A). Consistently, RT-PCR showed expression of shorter *IRE1B* mRNA in #2-5 and #9-6 seedlings (Fig. S5B). We expected that two isolated lines express N-terminally truncated IRE1B proteins by illegitimate translation (Makino *et al*, 2016), because translation from the original ATG produces premature N-terminal peptides (52 AA and 76 AA, respectively). These predicted ORFs in #2-5 and #9-6 have a truncated and an intact transmembrane domain, respectively (Fig. 7A). High sensitivity to Tm and DTT equivalent to *ire1a/b* were found in #2-5 and #9-6 lines compared to that in *ire1a/c* (Fig. 7B, S5C). Like the *ire1a/b* mutant, up- and down-regulation of *BiP3* and *PR-4* mRNA, respectively, by Tm treatment were diminished in #2-5 and #9-6 lines (Fig. 7C). Glycerol treatment-dependent

bZIP60 splicing as shown in *ire1a/c* was also diminished in #2-5 and #9-6 lines (Fig. 7D).

Nevertheless, mRNA expression of RIDD target genes in these lines was decreased as compared to those in *ire1a/b* under glycerol treatment (Fig. 7E, S6A). Growth defects and the reduction of seed set, which occurred in *ire1a/b ire1c/+* mutant, were not observed in the #2-5 and #9-6 plants (Fig. S6B, S6C).

Discussion

IRE1 is known as the most conserved and sole UPR signal transducer in lower eukaryotes (Mori, 2009). Evolution of multicellular organisms adapt IRE1 functions not only to environmental conditions but also to developmental conditions, as in the fact that IRE1 deficiency causes embryonic lethality in some organisms. In developmental processes, specific cells producing a large amount of secretory proteins, such as, β -cells of pancreas (Lee *et al*, 2011), goblet cells (Tsuru *et al*, 2013), and dendritic cells (Osorio *et al*, 2014), activate IRE1 in normal condition. These findings raise a question of whether production of unfolded proteins is prerequisite for the IRE1 activation in these specific cells. The present study showed that IRE1 activation without sensing unfolded protein is required for multifaceted developmental processes in Arabidopsis. We speculate that unfolded protein-independent IRE1 activation is a feature of anticipatory UPR (Vitale & Boston, 2008; Rutkowski & Hegde, 2010) to avoid producing ‘unprofitable’ unfolded proteins, as a primer for UPR, during the evolution of an unfolded protein-sensing system in multicellular organisms.

We found that plants heterozygous for the *IRE1C* allele (*ire1c/+*) in *ire1a/b* mutant background display developmental defects of male (and also probably female) gametogenesis, incomplete floral organ formation, and retardation of vegetative growth (Fig. 2). The incomplete dominance of the *IRE1C* allele is probably due to low expression of *IRE1C* transcript. The *IRE1C* expression is distinct in anther (Fig. S3A) and embryo (Fig. S3B), which is somewhat similar to that of *IRE1B* (Koizumi *et al*, 2001). Expression of *IRE1A* alone may be insufficient for proper Arabidopsis development because we could not obtain *ire1b ire1c* double mutant. Functions and physiological significance of the Arabidopsis *IRE1C* is still unclear. A closely related species, *Arabidopsis lyrata*, has four *IRE1* genes, *IRE1A* (XP_002884063), *IRE1B* (EFH48369), *IRE1C* (XP_002884871), and *IRE1C-like* (EFH64123). Amino acid sequence similarities between those in *A. thaliana* and *A. lyrata* are high in *IRE1A* (93%) and *IRE1B* (91%), whereas *IRE1C* proteins are more diversified (66%). *A. lyrata* also has *IRE1C-like* gene with low sequence similarity. These results suggest that these *IRE1C* genes probably arose through gene duplication during evolution of Brassicaceae species.

Pollen is known to be particularly sensitive to environmental conditions that disturb protein homeostasis (Fragkostefanakis *et al*, 2016). In high temperature, *ire1a/b* mutant displays male-sterility (Deng *et al*, 2016), suggesting that pollen development is sensitive to heat stress and that

IRE1-dependent UPR pathway is required for protecting male fertility from heat stress. This feature seems to be distinct from the requirement of the UPR-independent IRE1 activation for pollen development in unstressed condition observed in the present study. IRE1 activation in pollen without stress conditions was suggested by detection of bZIP60s in anther (Iwata *et al*, 2008), while *ire1a/b* mutant does not compromise pollen development under normal conditions (Deng *et al*, 2013, 2016). In the present study, we demonstrate that IRE1C, which lacks a sensor domain, acts redundantly with IRE1A and IRE1B in pollen development. Observation of the pollen development in *ire1a/b ire1c/+* mutant showed reduced number of pollen (Fig. 5) and abnormal tetrad (Fig. 4O), suggesting that male gametogenesis in the *ire1a/b/c* haplotype is defective in meiosis. Additionally, the *ire1a/b ire1c/+* mutant showed collapsed pollen grains at stage 11 (Fig. 5), which is somewhat similar to that observed in RNAi-mediated suppression of ER- and Golgi-located phospholipase A₂ transgenic plants (Kim *et al*, 2011). Together with the results that no transmission of *ire1c* allele were found through *ire1a/b* male gametophyte and that Δ LD can restore the transmission in the *ire1a/b/c* haplotype (Tables 1, 2), the unfolded protein-independent IRE1 activation is required for the male gametogenesis in unstressed conditions.

Genetic analysis also showed distorted segregation ratios in progenies of crosses between *ire1a/b ire1c/+* females and *ire1a/b* or wild-type males (Tables 1, 2), suggesting that the unfolded protein-independent IRE1 activation may be involved in embryogenesis or female gametogenesis. This hypothesis is supported by the observations that the sensor domain-lacking *IRE1B* mutant lines (i.e., #2-5 and #9-6) in *ire1a/c* background set seeds normally (Fig. S6C), and that *IRE1B* (Koizumi *et al*, 2001) and *IRE1C* (Fig. S3B) express in ovule and embryo, respectively. Inconsistent with the result of the #2-5 and #9-6 lines, we could not obtain homozygous *ire1c* mutant plants from selfed progenies of the *ire1a/b ire1c/+* plants expressing FLAG-IRE1B(WT) or Δ LD plants. A possible reconciliation could be that the *IRE1B* transgene promoter is not expressed in embryo at a level equivalent to endogenous *IRE1B* due to epigenetic modifications of the promoter or to insufficiency in the length of the transgene promoter.

By co-expression of two gRNAs and Cas9, part of *IRE1B*-coding regions (981 and 1,216 bp) corresponding to its sensor domain was removed from the *ire1a/c* mutant genome (Fig. 7A). It is inconceivable that illegitimate translation that results in sensor domain-lacking IRE1B (Fig. 7A) does not occur, because the *ire1a/b/c* mutant is lethal. *IRE1B* mRNA may be compatible with illegitimate translation because its 5'UTR contains uORF and *IRE1B* mRNA degradation by premature stop codon (Garneau *et al*, 2007) was not observed in #2-5 and #9-6 (Fig. S5B). Therefore, it is most conceivable that expression of sensor domain-lacking IRE1B confers normal seed set in #2-5 and #9-6. This unexpected IRE1 translation may also occur in known *ire1* null mutants in other organisms, such as *C. elegans ire1(v33)* mutant (Shen *et al*, 2001). Whether a shorter TM domain in #2-5 is functional at a transmembrane domain needs to be elucidated.

The present study shows distinct modes of IRE1 activation by saturated fatty acid *in vivo*.

Compared to Tm or DTT treatments (Mishiba *et al*, 2013), the level of IRE1 activation (i.e. fold induction of *bZIP60s* mRNA) by glycerol treatment was low. While full-length IRE1B activates both *bZIP60* splicing and RIDD under glycerol treatment, sensor domain-lacking IRE1B activates RIDD but not *bZIP60* splicing (Figs. 6, 7, S4, and S6). Biochemical studies in other model systems showed that oligomerization of IRE1 is required for XBP1/HAC1 cleavage but not RIDD (Tam *et al*, 2014). If plant IRE1 also acts in the same way, sensor domain-lacking IRE1 may be less likely to undergo oligomerization by saturated fatty acid. *In vivo* phosphorylation of FLAG-IRE1B was found under glycerol treatment (Fig. 6D), whereas phosphorylation of Δ LD is rather complicated. Since Δ LD exhibits multiple phosphorylation states and one of the state is stable regardless of stress (Fig. 6H), basal RIDD activity (Maurel *et al*, 2014) may exist in unstressed tissues. This hypothesis may explain growth retardation of *ire1a/b ire1c/+* plants (Fig. 2A) in unstressed conditions. Considering our current observations that Δ LD restores developmental defects found in the *ire1a/b ire1c/+* mutant and that deletion of the IRE1B's sensor domain in #2-5 and #9-6 does not prevent their development, RIDD activity may play an important role in the developmental processes. This hypothesis is partially supported by the findings of Deng *et al*, (2013) that *ire1a/b bzip28* but not *bzip60 bzip28* mutant haplotypes impaired male gametogenesis (note that bZIP28 is another UPR arm in Arabidopsis).

In conclusion, this study shows that the unfolded protein-independent IRE1 activation is involved in multifaceted developmental processes, especially pollen development, in Arabidopsis. We hypothesize that the alternative IRE1 activation pathway may be conserved in multicellular organisms as an 'anticipatory' mode (Walter & Ron, 2011; Shapiro *et al*, 2016) of the UPR to avoid producing unfolded proteins in differentiated cells synthesizing a large amount of secretory proteins.

Materials and Methods

Plant materials and stress treatments

Arabidopsis thaliana Col-0 ecotype and T-DNA insertion mutants in the Col-0 background were used in this study. Plants were grown on soil or half strength Murashige and Skoog (1/2 MS) medium containing 0.8% agar and 1% sucrose under 16 h light and 8 h dark conditions at 22°C. T-DNA insertion mutants of *ire1a*, *ire1b*, and *ire1a/b* were described previously (Nagashima *et al*, 2011). A T-DNA insertion mutant of *IRE1C* (SALK_204405) was obtained from the Arabidopsis Biological Resource Center. T-DNA insertions were confirmed by genomic PCR as shown in Fig. S1A and S1B using primers listed in Table S1. Extraction of DNA for genotyping was carried out as described by Kasajima *et al*. (2004). Genotyping PCR was performed using KAPA Taq Extra PCR kit (Kapa Biosystems) according to the manufacturer's protocol. To test the sensitivity of seedlings to Tm and DTT, sterilized seeds were sown on a 1/2 MS plate containing Tm (0.1 μ g/mL) or DTT (1 mM). For stress treatments, 10-d-old seedlings in 1/2 MS liquid medium (Nagashima *et al*, 2011) were treated

with 5 μ g/mL Tm, 1 mM DTT, or DMSO (mock) for 1 to 5 h. For glycerol treatment, 7-d-old seedlings in liquid medium were treated with 50 mM glycerol for 3 d followed by treatment with 0.6 mM cordycepin (Wako) for 0 to 5 h.

Production of transgenic Arabidopsis plants

For *IRE1C* promoter-*GUS* fusion construct, a 1,577-bp fragment of the *IRE1C* promoter was cloned into pENTR/D-TOPO (Thermo Fisher Scientific) and transferred into pSMAB-GW-*GUS* (Fig. S2A) binary vector by Gateway LR reaction (Thermo Fisher Scientific). For FLAG-tagged *IRE1* constructs, 5,126 and 5,081 bp fragments of *IRE1A* and *IRE1B* genes, respectively, comprising approximately 0.9 and 1.2 kb of their promoter regions, respectively, were amplified by PCR with primers listed in Table S1 and cloned into pENTR/D-TOPO. Triple FLAG-tag and mutations in the kinase and RNase domains were introduced by PCR. These pENTR vectors were transferred into pSMAB-GW destination binary vector (Fig. S2B) by Gateway LR reaction. The Δ LD-expressing vector was made by partial *Mlu*I digestion of pSMAB-FLAG-*IRE1B*(WT) followed by *Nhe*I digestion, blunt end formation by T4 DNA polymerase, and self-ligation. For CRISPR/Cas9, we used pKIR1.0 binary vector (Tsutsui & Higashiyama, 2017) comprising AtU6 promoter-driven gRNA1 and AtU6 promoter-driven gRNA2 (Fig. S2C). The target sequences of the gRNA1 and gRNA2 are listed in Table S1. The binary vectors were introduced into *Rhizobium* strain EHA101 (Hood *et al*, 1986) and transformed into *ire1a/b* (for *IRE1A* and *IRE1B* constructs), *ire1a/c* (for CRISPR/Cas9) mutants, and wild-type (for *IRE1C* promoter-*GUS*) by the floral dip method (Clough & Bent, 1998).

RNA analysis

Total RNA was extracted using a NucleoSpin RNA kit (Takara) according to the manufacturer's protocol. For RT-PCR and qPCR, 500 ng of RNA was subjected to reverse transcription with random primers using High Capacity cDNA Reverse Transcription Kit (Thermo Fisher Scientific) according to the manufacturer's protocol. qPCR was performed with an ABI 7300 Real-Time PCR System (Applied Biosystems) using Thunderbird SYBR qPCR Mix (Toyobo), and the transcript abundance of the target genes were normalized to that of 18S rRNA (Zoschke *et al*, 2007). Primers used for RT-PCR and qPCR are listed in Table S1. RNA gel blot analysis was conducted using DIG High Prime DNA Labeling and Detection Starter Kit II (Roche) according to the manufacturer's protocol. Primers used to generate probes are listed in Table S1.

Protein analysis

Total protein extraction from Arabidopsis seedlings was performed as described by Liu *et al* (2011). Protein extracts were fractionated by SDS-PAGE followed by western blotting with HRP-conjugated anti-FLAG antibody (PM020-7; MBL; 1:10,000) and chemiluminescent detection using Chemi-Lumi One Ultra (Nacalai Tesque). To reveal Rubisco large subunit, Coomassie Brilliant Blue (CBB) staining

of the gel or Ponceau-S staining of the membrane were performed. For Phos-tag SDS-PAGE (Kinoshita & Kinoshita-Kikuta, 2011), 6% polyacrylamide gels containing 5-15 μ M Phos-tag acrylamide (Wako) and 10-30 μ M $ZnCl_2$ were run according to the manufacturer's protocol. For Phos-tag SDS-PAGE sample preparation, Arabidopsis seedlings was ground in liquid nitrogen and homogenized in an extraction buffer (100 mM Tris-HCl, pH 7.5, 0.25 M sucrose, 5 mM PMSF). The homogenate was centrifuged at 2,000 $\times g$ for 2 min (4°C) and the supernatant was centrifuged at 10,000 $\times g$ for 2 min (4°C). The supernatant was further centrifuged at 100,000 $\times g$ for 30 min (4°C). The crude microsomal fraction pellet was subjected to the protein extraction as described above.

Histological analysis

Anther samples were fixed with 4% glutaraldehyde in 60 mM HEPES (pH 7.0) containing 0.125 M sucrose. After dehydration in a graded series of ethanol/water mixtures, the samples were embedded in Quetol 651 resin (Nisshin EM) with formulation for plant material (Ellis, 2016). Semi-thin (2 μ m) transverse sections were prepared from at least eight resin blocks per sample and stained with 0.2% toluidine blue. Stained sections were examined using a BZ-9000 microscope (Keyence). Histochemical GUS staining of *IRE1C* promoter-*GUS* plants was performed as previously described (Iwata *et al*, 2008).

Fatty acid analysis

Arabidopsis seedlings (approx. 150 mg FW) at 10 DAG was used for the analysis of fatty acid composition. The fatty acids extracted with hexane were methylated and purified with fatty acid methylation kit (Nacalai Tesque) following the manufacturer's instructions. The fatty acid compositions were determined using an Agilent 6890 gas chromatograph (Agilent Technologies) equipped with a DB-23 column (30 m \times 0.25 mm \times 0.25 μ m; Agilent Technologies). Nonadecanoic methyl ester (C19:0) was used as the internal standard.

Acknowledgements

We thank Ms. Ayumi Sakei, Ms. Fumika Yagi, Ms. Sae Saito (Osaka Prefecture University), and Dr. Yukihiro Nagashima (Texas A&M University) for technical assistance. We also thank the ABRC and GABI-Kat for providing T-DNA insertion lines, Dr. Hiroki Tsutsui and Dr. Tetsuya Higashiyama (Nagoya University) for pKIR1.0. This work was supported by Grant-in-Aid for Scientific Research (26450010, 17K07610) from The Ministry of Education, Culture, Sports, Science and Technology (MEXT), Shorai Foundation for Science and Technology, and Takeda Science Foundation.

Author contributions

KiM directed the project. KiM and NK design the experiments. KiM, YI, RH and NN produced transgenic plants. TM and KiM performed histological analysis. AM performed fatty acid analysis. KiM performed all other experiments. KiM and YI provided the materials and reagents. KiM, YI, and NK wrote the manuscript. All authors have read and approved the manuscript.

Conflict of interest

The authors declare that they have no conflict of interest.

References

- Chen Y, Brandizzi F (2012) AtIRE1A/AtIRE1B and AGB1 independently control two essential unfolded protein response pathways in Arabidopsis. *Plant J* 69: 266–277
- Clough SJ, Bent AF (1998) Floral dip: a simplified method for agrobacterium-mediated transformation of *Arabidopsis thaliana*. *Plant J* 16: 735–743
- Deng Y, Humbert S, Liu JX, Srivastava R, Rothstein SJ, Howell SH (2011) Heat induces the splicing by IRE1 of a mRNA encoding a transcription factor involved in the unfolded protein response in Arabidopsis. *Proc Natl Acad Sci USA* 108: 7247–7252
- Deng Y, Srivastava R, Quilichini TD, Dong H, Bao Y, Horner HT, Howell SH (2011) IRE1, a component of the unfolded protein response signaling pathway, protects pollen development in Arabidopsis from heat stress. *Plant J* 88: 193–204
- Deng Y, Srivastava R, Howell SH (2013) Protein kinase and ribonuclease domains of IRE1 confer stress tolerance, vegetative growth, and reproductive development in Arabidopsis. *Proc Natl Acad Sci USA* 110: 19633–19638
- Ellis EA (2016) Quetol 651: Not just a low viscosity resin. *Microsc Res Techniq* 79: 50–57
- Fragkostefanakis S, Mesihovic A, Hu Y, Schleiff E (2016) Unfolded protein response in pollen development and heat stress tolerance. *Plant Reprod* 29: 81–91
- Garneau NL, Wilusz J, Wilusz CJ (2007) The highways and byways of mRNA decay. *Nat Rev Mol Cell Biol* 8: 113–126
- Halbleib K, Pesek K, Covino R, Hofbauer HF, Wunnicke D, Hänelt I, Hummer G, Ernst R (2017) Activation of the unfolded protein response by lipid bilayer stress. *Mol Cell* 67: 673–684
- Han D, Lerner AG, Vande Walle L, Upton JP, Xu W, Hagen A, Backes BJ, Oakes SA, Papa FR (2009) IRE1 α kinase activation modes control alternate endoribonuclease outputs to determine divergent cell fates. *Cell* 138: 562–575
- Hayashi S, Wakasa Y, Ozawa K, Takaiwa F (2016) Characterization of IRE1 ribonuclease-mediated mRNA decay in plants using transient expression analyses in rice protoplasts. *New Phytol* 210:

- 1259–1268
- Hollien J, Weissman JS (2006) Decay of endoplasmic reticulum-localized mRNAs during the unfolded protein response. *Science* 313: 104–107
- Hollien J, Lin JH, Li H, Stevens N, Walter P, Weissman JS (2009) Regulated Ire1-dependent decay of messenger RNAs in mammalian cells. *J Cell Biol* 186: 323–331
- Hood EE, Helmer GL, Fraley RT, Chilton MD (1986) The hypervirulence of *Agrobacterium tumefaciens* A281 is encoded in a region of pTiBo542 outside of TDNA. *J Bacteriol* 168: 1291–1301
- Hou NS, Gutschmidt A, Choi DY, Pather K, Shi X, Watts JL, Hoppe T, Taubert S (2014) Activation of the endoplasmic reticulum unfolded protein response by lipid disequilibrium without disturbed proteostasis in vivo. *Proc Natl Acad Sci USA* 111: E2271–E2280
- Iqbal J, Dai K, Seimon T, Jungreis R, Oyadomari M, Kuriakose G, Ron D, Tabas I, Hussain MM (2008) IRE1 β inhibits chylomicron production by selectively degrading MTP mRNA. *Cell Metab* 7: 445–455
- Iwata Y, Koizumi N (2005) An *Arabidopsis* transcription factor, AtbZIP60, regulates the endoplasmic reticulum stress response in a manner unique to plants. *Proc Natl Acad Sci USA* 102: 5280–5285
- Iwata Y, Fedoroff NV, Koizumi N (2008) *Arabidopsis* bZIP60 is a proteolysis-activated transcription factor involved in the endoplasmic reticulum stress response. *Plant Cell* 20: 3107–3121
- Iwata Y, Hayashi N, Tabara K, Mishiba KI, Koizumi N (2016) Tunicamycin-induced inhibition of protein secretion into culture medium of *Arabidopsis* T87 suspension cells through mRNA degradation on the endoplasmic reticulum. *Biosci Biotechnol Biochem* 80: 1168–1171
- Kachroo A, Venugopal SC, Lapchuk L, Falcone D, Hildebrand D, Kachroo P (2004) Oleic acid levels regulated by glycerolipid metabolism modulate defense gene expression in *Arabidopsis*. *Proc Natl Acad Sci USA* 101: 5152–5157
- Kasajima I, Ide Y, Ohkama-Ohtsu N, Hayashi H, Yoneyama T, Fujiwara T (2004) A protocol for rapid DNA extraction from *Arabidopsis thaliana* for PCR analysis. *Plant Mol Biol Rep* 22: 49–52
- Kim HJ, Ok SH, Bahn SC, Jang J, Oh SA, Park SK, Twell D, Ryu SB, Shin JS (2011) Endoplasmic reticulum- and golgi-localized phospholipase A₂ plays critical roles in *Arabidopsis* pollen development and germination. *Plant Cell* 23: 94–110
- Kimmig P, Diaz M, Zheng J, Williams CC, Lang A, Aragón T, Li H, Walter P (2012) The unfolded protein response in fission yeast modulates stability of select mRNAs to maintain protein homeostasis. *eLife* 1: e00048
- Kinoshita E, Kinoshita-Kikuta E (2011) Improved Phos-tag SDS-PAGE under neutral pH conditions for advanced protein phosphorylation profiling. *Proteomics* 11: 319–323.
- Koizumi N, Martinez IM, Kimata Y, Kohno K, Sano H, Chrispeels MJ (2001) Molecular characterization of two *Arabidopsis* Ire1 homologs, endoplasmic reticulum-located transmembrane protein kinases. *Plant Physiol* 127: 949–962

- Lee AH, Heidtman K, Hotamisligil GS, Glimcher LH (2011) Dual and opposing roles of the unfolded protein response regulated by IRE1 α and XBP1 in proinsulin processing and insulin secretion. *Proc Natl Acad Sci USA* 108: 8885–8890
- Liu L, Cui F, Li Q, Yin B, Zhang H, Lin B, Wu Y, Xia R, Tang S, Xie Q (2011) The endoplasmic reticulum-associated degradation is necessary for plant salt tolerance. *Cell Res* 21: 957–969
- Makino S, Fukumura R, Gondo Y (2016) Illegitimate translation causes unexpected gene expression from on-target out-of-frame alleles created by CRISPR-Cas9. *Sci Rep* 6: 39608
- Maurel M, Chevet E, Tavernier J, Gerlo S (2014) Getting RIDD of RNA: IRE1 in cell fate regulation. *Trends Biochem Sci* 39: 245–254
- Mishiba KI, Nagashima Y, Suzuki E, Hayashi N, Ogata Y, Shimada Y, Koizumi N (2013) Defects in IRE1 enhance cell death and fail to degrade mRNAs encoding secretory pathway proteins in the *Arabidopsis* unfolded protein response. *Proc Natl Acad Sci USA* 110: 5713–5718
- Mori K (2009) Signaling pathways in the unfolded protein response: development from yeast to mammals. *J Biochem* 146: 743–750
- Nagashima Y, Mishiba KI, Suzuki E, Shimada Y, Iwata Y, Koizumi N (2011) Arabidopsis IRE1 catalyses unconventional splicing of *bZIP60* mRNA to produce the active transcription factor. *Sci Rep* 1: 29
- Nikawa JI, Yamashita S (1992) *IRE1* encodes a putative protein kinase containing a membrane-spanning domain and is required for inositol phototrophy in *Saccharomyces cerevisiae*. *Mol Microbiol* 6: 1441–1446
- Osorio F, Tavernier SJ, Hoffmann E, Saeys Y, Martens L, Veters J, Delrue I, De Rycke R, Parthoens E, Pouliot P, Iwawaki T, Janssens S, Lambrecht BN (2014) The unfolded-protein-response sensor IRE-1 α regulates the function of CD8 α^+ dendritic cells. *Nat Immunol* 15:248–257
- Promlek T, Ishiwata-Kimata Y, Shido M, Sakuramoto M, Kohno K, Kimata Y (2011) Membrane aberrancy and unfolded proteins activate the endoplasmic reticulum stress sensor Ire1 in different ways. *Mol Biol Cell* 22: 3520–3532
- Rutkowski DT, Hegde RS (2010) Regulation of basal cellular physiology by the homeostatic unfolded protein response. *J Cell Biol* 189: 783–794
- Ryoo HD, Li J, Kang MJ (2013) *Drosophila* XBP1 expression reporter marks cells under endoplasmic reticulum stress and with high protein secretory load. *PLOS ONE* 8: e75774
- Shapiro DJ, Livezey M, Yu L, Zheng X, Andruska N (2016) Anticipatory UPR activation: a protective pathway and target in cancer. *Trends Endocrin Met* 27: 731–741
- Shen X, Ellis RE, Lee K, Liu CY, Yang K, Solomon A, Yoshida H, Morimoto R, Kurnit DM, Mori K, Kaufman RJ (2001) Complementary signaling pathways regulate the unfolded protein response and are required for *C. elegans* development. *Cell* 107: 893–903
- Sidrauski C, Walter P (1997) The transmembrane kinase Ire1p is a site-specific endonuclease that initiates mRNA splicing in the unfolded protein response. *Cell* 90: 1031–1039

- Smyth DR, Bowman JL, Meyerowitz EM (1990) Early flower development in *Arabidopsis*. *Plant Cell* 2: 755–767
- Tam AB, Koong AC, Niwa M (2014) Ire1 has distinct catalytic mechanisms for *XBP1/HAC1* splicing and RIDD. *Cell Rep* 9: 850–858
- Tamura K, Stecher G, Peterson D, Filipinski A, Kumar S (2013) MEGA6: molecular evolutionary genetics analysis version 6.0. *Mol Biol Evol* 30: 2725–2729
- Tsuru A, Fujimoto N, Takahashi S, Saito M, Nakamura D, Iwano M, Iwawaki T, Kadokura H, Ron D, Kohno K (2013) Negative feedback by IRE1 β optimizes mucin production in goblet cells. *Proc Natl Acad Sci USA* 110: 2864–2869
- Tsutsui H, Higashiyama T (2017) pKAMA-ITACHI vectors for highly efficient CRISPR/Cas9-mediated gene knockout in *Arabidopsis thaliana*. *Plant Cell Physiol* 58: 46–56
- Vitale A, Boston RS (2008) Endoplasmic reticulum quality control and the unfolded protein response: insights from plants. *Traffic* 9: 1581–1588
- Volmer R, van der Ploeg K, Ron D (2015) Membrane lipid saturation activates endoplasmic reticulum unfolded protein response transducers through their transmembrane domains. *Proc Natl Acad Sci USA* 110: 4628–4633
- Volmer R, Ron D (2015) Lipid-dependent regulation of the unfolded protein response. *Curr Opin Cell Biol* 33: 67–73
- Wakasa Y, Hayashi S, Ozawa K, Takaiwa F (2012) Multiple roles of the ER stress sensor IRE1 demonstrated by gene targeting in rice. *Sci Rep* 2: 944
- Walter P, Ron D (2011) The unfolded protein response: from stress pathway to homeostatic regulation. *Science* 334: 1081–1086
- Yang L, Xue Z, He Y, Sun S, Chen H, Qi L (2010) A Phos-tag-based approach reveals the extent of physiological endoplasmic reticulum stress. *PLOS ONE* 5: e11621
- Yoshida H, Matsui T, Yamamoto A, Okada T, Mori K (2001) XBP1 mRNA is induced by ATF6 and spliced by IRE1 in response to ER stress to produce a highly active transcription factor. *Cell* 107: 881–891
- Zhang K, Wong HN, Song B, Miller CN, Scheuner D, Kaufman RJ (2005) The unfolded protein response sensor IRE1 α is required at 2 distinct steps in B cell lymphopoiesis. *J Clin Invest* 115: 268–281
- Zoschke R, Liere K, Börner T (2007) From seedling to mature plant: *Arabidopsis* plastidial genome copy number, RNA accumulation and transcription are differentially regulated during leaf development. *Plant J* 50: 710–722

Figure Legends

Figure 1. Arabidopsis IRE1C does not contribute to the unfolded protein response. (A)

Structures of Arabidopsis IRE1A, IRE1B and IRE1C proteins. SS, signal sequence; TM, transmembrane domain. (B) Phylogenetic tree of IRE1-like proteins from mammals (*Homo sapiens*), fungi (*Saccharomyces cerevisiae* and *Saccharomyces pombe*) and plants was constructed by UPGMA using MEGA 6 (Tamura *et al*, 2013). The tree is drawn to scale, with branch lengths in the same units as those of the evolutionary distances used to infer the phylogenetic tree. The evolutionary distances were computed using the Poisson correction method and are in the units of the number of amino acid substitutions per site. (C) Wild-type (WT) and *ire1* mutant plants 40 days after germination (DAG). Bar = 10 mm. (D) DTT sensitivity of the *ire1* mutants. Seedlings at 15 DAG of the indicated lines were treated with or without 1 mM DTT. (E) RNA blot analysis of *BiP3* and *PR-4* in WT and *ire1* mutants. Seedlings at 10 DAG were treated with (+) or without (-) 5 mg/l tunicamycin (Tm) for 5 h.

Figure 2. *ire1a ire1b* homozygous and *ire1c* heterozygous plants show developmental defects.

(A) Self-pollinated progenies of *ire1a ire1b ire1c/+* mutant plants at 40 DAG. Genotypes were shown on the left. Bar = 10 mm. (B) Siliques of *ire1a ire1b ire1c/+* (left) and *ire1a ire1b +/+* (right) plants. Bar = 10 mm. (C) Reproductive development of *ire1* mutants. Flowers at stage 14 (Smyth *et al*, 1990; upper; bar = 1 mm), siliques (middle; bar = 3 mm), and anthers at stage 12 stained with Alexander's stain (lower; bar = 100 μ m) from wild-type (WT) and *ire1* mutants were shown.

Figure 3. Transgenic *ire1a ire1b* plants expressing FLAG-tagged wild-type or mutant IRE1.

(A) Schema of FLAG-tagged IRE1 proteins. Mutations of kinase and RNase domains are shown as arrowheads. SS, signal sequence; TM, transmembrane domain. (B) Detection of FLAG-IRE1 proteins in the transgenic *ire1a ire1b* plants with anti-FLAG antibody. Ponceau S or CBB staining was used as loading control. (C) RNA blot analysis of *BiP3* and *PR-4* in wild-type (WT), *ire1a ire1b* mutant and transgenic *ire1a ire1b* plants. Seedlings at 10 DAG were treated with (+) or without (-) 5 mg/l tunicamycin (Tm) for 5 h. (D) Detection of FLAG-IRE1B(WT) and FLAG-IRE1B(K487A) with anti-FLAG antibody in the transgenic *ire1a ire1b* plants treated with Tm or DTT. Samples were resolved on Phos-tag SDS-PAGE to detect the phosphorylated FLAG-IRE1B (p-IRE1B). (E) DTT sensitivity of the transgenic *ire1a ire1b* plants. Seedlings at 15 DAG of the indicated lines were treated with or without 1 mM DTT.

Figure 4. Phenotypic complementation of *ire1a ire1b ire1c/+* mutants by FLAG-IRE1B(WT) or Δ LD.

Phenotypes of the transgenic *ire1a ire1b ire1c/+* plant having FLAG-IRE1B(WT) (left), Δ LD (center) and *ire1a ire1b ire1c/+* plant (right). (A-C) Plants at 40 DAG. Bar = 10 mm. (D-F) Flowers at stage 14. Bar = 500 μ m. (G-I) Siliques. Bar = 3 mm. (J-L) Anthers at stage 12 stained with Alexander's stain. Bar = 100 μ m. (M-O) Tetrads stained with toluidine blue. Bar = 20 μ m.

Figure 5. Abnormal pollen development in *ire1a ire1b ire1c/+* is partially complemented by Δ LD. Transverse sections of developing anthers at stages 8, 9, 11 in WT (left), *ire1a ire1b ire1c/+* mutant (middle) and transgenic *ire1a ire1b ire1c/+* plants having Δ LD (right). Arrowheads indicate collapsed pollen grains. Bar = 50 μ m.

Figure 6. Glycerol treatment stimulates IRE1 kinase and RNase activities. (A) Percentages of saturated fatty acids (16:0 and 18:0) in WT and *ire1a ire1b* plants at 10 DAG treated with (G) or without (C) glycerol for 3 d. Error bars represent SD (n = 6). (B, C) Detection of *bZIP60* mRNA splicing in WT, *ire1a ire1b* plants (B) and FLAG-IRE1 transgenic *ire1a ire1b* plants (C) at 10 DAG. RT-PCR was performed using *bZIP60s*-specific primers. *Actin2* (*Act2*) was used as an internal control. (B) Glycerol treatment was performed for 0-4 d. (C) Plants were treated with (+) or without (-) glycerol for 3 d. (D) Detection of FLAG-IRE1B(WT) with anti-FLAG antibody in the transgenic *ire1a ire1b* plants treated with glycerol for 0-3 d. Samples were resolved on SDS-PAGE (upper) and Phos-tag SDS-PAGE (lower) followed by immunodetection with anti-FLAG antibody. An equal loading was shown by CBB staining following SDS-PAGE (middle). (E, F) RNA blot analysis of *PR-4*, *PRX34* and/or *MBL1* in WT, *ire1a ire1b* plants (E) and FLAG-IRE1 transgenic *ire1a ire1b* plants (F) at 10 DAG. (E) Plants were treated with or without glycerol for 3 d and plants at 10 DAG were treated with cordycepin (Cord) for 0-5 h. (F) Three days of glycerol-treated plants at 10 DAG were treated with Cord for 0-2 h. (G, H) Detection of Δ LD with anti-FLAG antibody in the transgenic *ire1a ire1b* plants treated with glycerol, Tm or DTT. (G) Samples were resolved on SDS-PAGE followed by immunodetection with anti-FLAG antibody. CBB staining was used as loading control. (H) Samples were resolved on Phos-tag SDS-PAGE to detect the phosphorylated Δ LD (p- Δ LD). AP, alkaline phosphatase-treated sample. Asterisks indicate possible degradation products of Δ LD.

Figure 7. CRISPR/Cas9-mediated IREB gene editing in *ire1a ire1c* mutant. (A) Schema of hypothetical IRE1B products in the *IRE1B*-mutated *ire1a ire1c* T₃ plant lines #2-5 and #1-10. Positions of gRNA target sites are shown as arrowheads. SS, signal sequence; TM, transmembrane domain. (B) Tm sensitivity of the *ire1a ire1b*, *ire1a ire1c*, and *IRE1B*-mutated *ire1a ire1c* plants. Seedlings at 15 DAG of the indicated lines were treated with or without 0.1 mg/l Tm. (C) RNA blot analysis of *BiP3* and *PR-4* in WT, *ire1a ire1b*, *ire1a ire1c* mutant and *IRE1B*-mutated *ire1a ire1c* plants. Seedlings at 10 DAG were treated with (+) or without (-) 5 mg/l tunicamycin (Tm) for 5 h. (D) Detection of *bZIP60* mRNA splicing in WT, *ire1a ire1b*, *ire1a ire1c*, and *IRE1B*-mutated *ire1a ire1c* plants at 10 DAG treated with (+) or without (-) glycerol for 3 d. (E) RNA blot analysis of *PR-4* and *PRX34* in WT, *ire1a ire1b*, *ire1a ire1c*, and *IRE1B*-mutated *ire1a ire1c* plants at 10 DAG treated with glycerol for 3 d. The samples were treated with (+) or without (-) Cord for 2 h immediately before sampling.

Figure Legends for Supplementary Materials

Figure S1. Genotyping of *IRE1* genes in *ire1* mutants. (A) Schematic representation of T-DNA insertion sites in *ire1a*, *ire1b*, and *ire1c*. Grey and white boxes indicate coding sequences and untranslated regions, respectively. Arrows indicate the positions of primers (Table S1) used for genotyping. (B) Genotyping of wild-type, *ire1a*, *ire1b*, *ire1c*, *ire1a ire1b*, *ire1a ire1c*, and selfed siblings (*ire1c/+* or *+/+*) of *ire1a ire1b ire1c/+*. Lanes 1-3, three independent plants for each mutant. Lane M, 100 bp DNA ladder. M, mutant. W, wild-type.

Figure S2. T-DNA constructs of the binary vectors used in this study. (A) *IRE1C* promoter-driven *GUS* reporter gene construct. *IRE1C* promoter region within pENTR vector was transferred into pSMAB-GW-*GUS* binary vector through Gateway LR reaction. (B) FLAG-tagged *IRE1A* and *IRE1B* constructs. Genomic regions of the *IRE1A* and *IRE1B* genes were cloned into pENTR vector and transferred into pSMAB-GW binary vector. Modifications are indicated in each panel. (C) A CRISPR/Cas9 binary vector containing gRNA1 and gRNA2 targeting the sensor domain of the *IRE1B* gene (see Fig. 7A).

Figure S3. Tissue-specific expression of *IRE1C* gene. (A-C) *GUS* histochemical staining of transgenic *Arabidopsis* containing *IRE1C* promoter-*GUS* fusion construct in floral tissues (A), ovules and embryo (B). Bar = 100 μ m. (C) 8-d-old seedlings treated with or without tunicamycin (Tm) for 5 h, and 11-d-old seedlings treated with glycerol for 3d. Bar = 5 mm.

Figure S4. Effect of RNase and sensor domain of *IRE1B* on *bZIP60* splicing and RIDD under glycerol treatment. (A) Detection of *bZIP60s* mRNA splicing in WT, *ire1a ire1b*, and FLAG-*IRE1B*(WT, Δ LD) transgenic *ire1a ire1b* plants at 10 DAG. RT-PCR was performed using *bZIP60s*-specific primers. *Actin2* (*Act2*) was used as an internal control. Glycerol treatment was performed for 0, 1, and 3 d. (B-D) The relative mRNA levels of *bZIP60s* (B), cytosolic marker protein genes (C), and RIDD target genes (D) in WT, *ire1a ire1b*, and FLAG-*IRE1B*(WT, K821A, Δ LD) transgenic *ire1a ire1b* plants. RNA from seedlings at 10 DAG treated with (+) or without (-) glycerol for 3 d was subjected to qPCR. Data are means \pm SEM of four independent experiments. Different letters within each treatment indicate significant differences ($P < 0.05$) by the Tukey-Kramer HSD test.

Figure S5. Characteristics of the CRISPR/Cas9-mediated *IRE1B* mutant lines #2-5 and #9-6. (A) Genotyping of *IRE1A-C* genes in wild-type, *ire1a ire1b*, *ire1a ire1c* mutants, and T₃ plants of lines #2-5 and #9-6. Lane M, 100 bp DNA ladder. Lanes 1-6, six independent plants for each line. M, mutant. W, wild-type. Note that PCR amplification of *Cas9* gene was performed to detect T-DNA, and

that #9-6 lane 7 is a T₂ sibling plant having T-DNA used as a control. (B) RT-PCR of *IRE1B* mRNA in *ire1a ire1c*, *ire1a ire1b* mutants, and T₃ plants of #2-5 and #9-6. *Actin2* (*Act2*) was used as an internal control. (C) DTT sensitivity of the *ire1a ire1b*, *ire1a ire1c* mutants, and T₃ plants of #2-5 and #9-6. Seedlings at 15 DAG were treated with or without 1mM DTT.

Figure S6. #2-5 and #9-6 lines retain RIDD activity and show no phenotypic abnormality. (A) The relative mRNA levels of RIDD target genes in WT, *ire1a ire1b*, *ire1a ire1c*, and *ire1a ire1c* with *IRE1B* mutation T₃ lines #2-5 and #9-6. RNA from seedlings at 10 DAG treated with glycerol for 3 d was subjected to qPCR. Data are means ± SEM of four independent experiments. Different letters indicate significant differences (P < 0.05) by the Tukey–Kramer HSD test. (B) T₃ plants of lines #2-5 and #9-6 and *ire1a ire1b ire1c/+* mutant at 40 DAG. Bar = 10 mm. (C) Siliques of the lines #2-5 (left) and #9-6 (right) plants. Bar = 3 mm.

Table 1. Transmission of the *ire1c* allele through the male and female gametophytes in the progenies of the *ire1a ire1b ire1c/+* mutants crossed with the *ire1a ire1b* mutant or self-pollinated.

Parental genotype		Genotypes of progeny				Observed ratio	Expected ratio
Female	Male	+/+	c/+	c/c	Total	+/+ : c/+ : c/c	+/+ : c/+ : c/c
<i>a/a b/b c/+</i>	<i>a/a b/b c/+</i>	83	25	0	108	1.0 : 0.30 : 0 ^a	1 : 2 : 1
<i>a/a b/b c/+</i>	<i>a/a b/b +/+</i>	186	39	0	225	1.0 : 0.21 : 0 ^a	1 : 1 : 0
<i>a/a b/b +/+</i>	<i>a/a b/b c/+</i>	119	0	0	119	119 : 0 : 0 ^a	1 : 1 : 0

^aSignificantly different from the Mendelian segregation ratio (χ^2 , $P < 0.01$)
 +, wild-type allele; a, *ire1a* allele; b, *ire1b* allele; c, *ire1c* allele

Table 2. Transmission of the *ire1c* allele through the male and female gametophytes in the progenies of the *ire1a ire1b ire1c/+* mutants having *IRE1B* or ΔLD transgenes crossed with the wild-type or self-pollinated.

Parental genotype		Genotypes of progeny				Observed ratio	Expected ratio
Female	Male	+/+	c/+	c/c	Total	+/+ : c/+ : c/c	+/+ : c/+ : c/c
+/+ +/+ +/+	<i>a/a b/b c/+</i>	202	0	0	202	202 : 0 : 0 ^a	1 : 1 : 0
+/+ +/+ +/+	<i>a/a b/b c/+ IRE1B</i>	43	14	0	57	1.0 : 0.33 : 0 ^a	1 : 1 : 0
+/+ +/+ +/+	<i>a/a b/b c/+ ΔLD</i>	60	34	0	94	1.0 : 0.57 : 0 ^a	1 : 1 : 0
<i>a/a b/b c/+</i>	+/+ +/+ +/+	266	81	0	347	1.0 : 0.30 : 0 ^a	1 : 1 : 0
<i>a/a b/b c/+ IRE1B</i>	+/+ +/+ +/+	130	32	0	162	1.0 : 0.25 : 0 ^a	1 : 1 : 0
<i>a/a b/b c/+ ΔLD</i>	+/+ +/+ +/+	135	25	0	160	1.0 : 0.19 : 0 ^a	1 : 1 : 0
<i>a/a b/b c/+ IRE1B</i>	<i>a/a b/b c/+ IRE1B</i>	53	101	0	154	1.0 : 1.9 : 0 ^a	1 : 2 : 1
<i>a/a b/b c/+ ΔLD</i>	<i>a/a b/b c/+ ΔLD</i>	97	140	0	237	1.0 : 1.4 : 0 ^a	1 : 2 : 1

^aSignificantly different from the Mendelian segregation ratio (χ^2 , P<0.01)

+, wild-type allele; a, *ire1a* allele; b, *ire1b* allele; c, *ire1c* allele; *IRE1B*, *FLAG-IRE1B(WT)* transgene (homozygote); ΔLD , ΔLD transgene (homozygote)

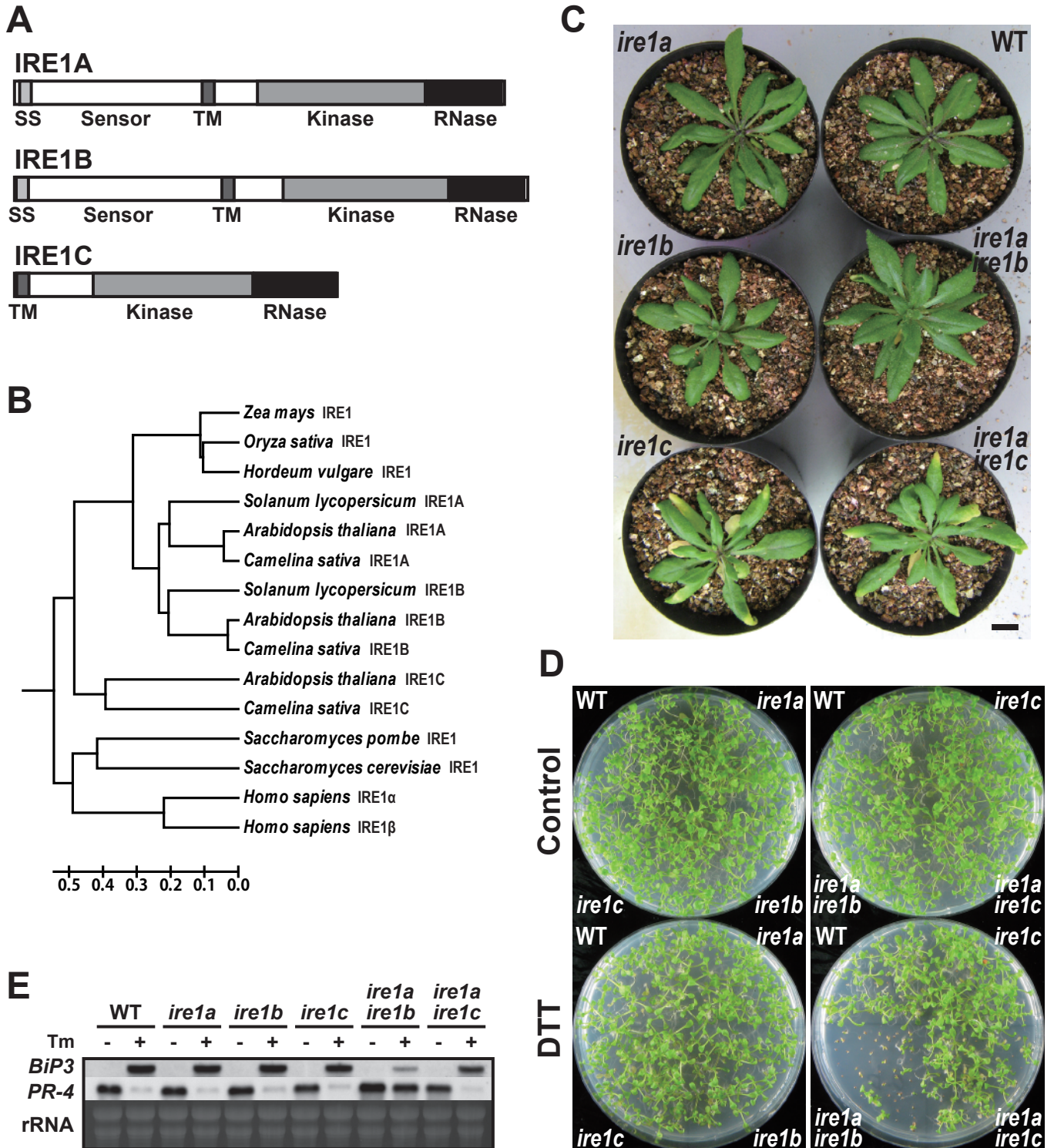


Figure 1

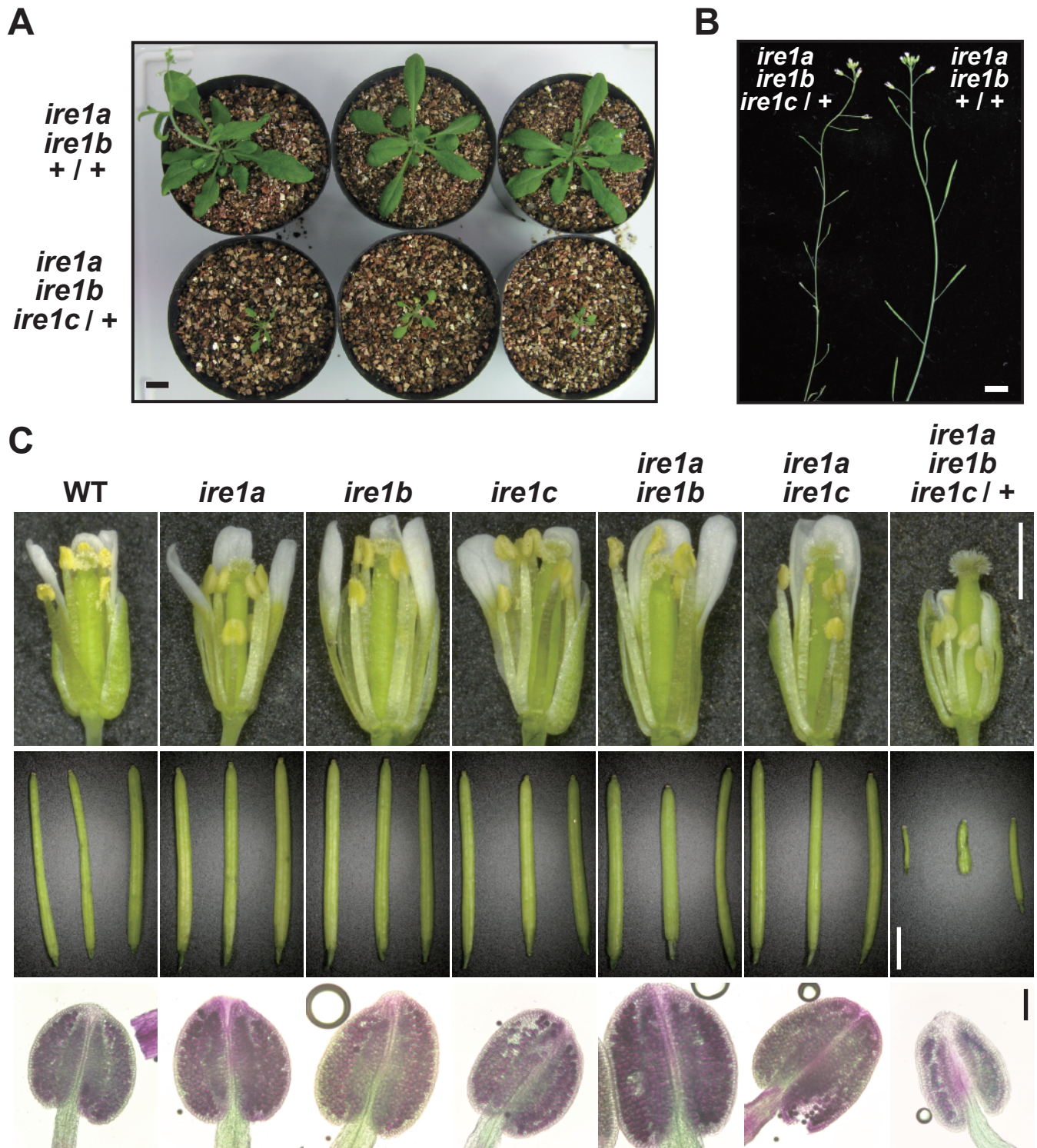


Figure 2

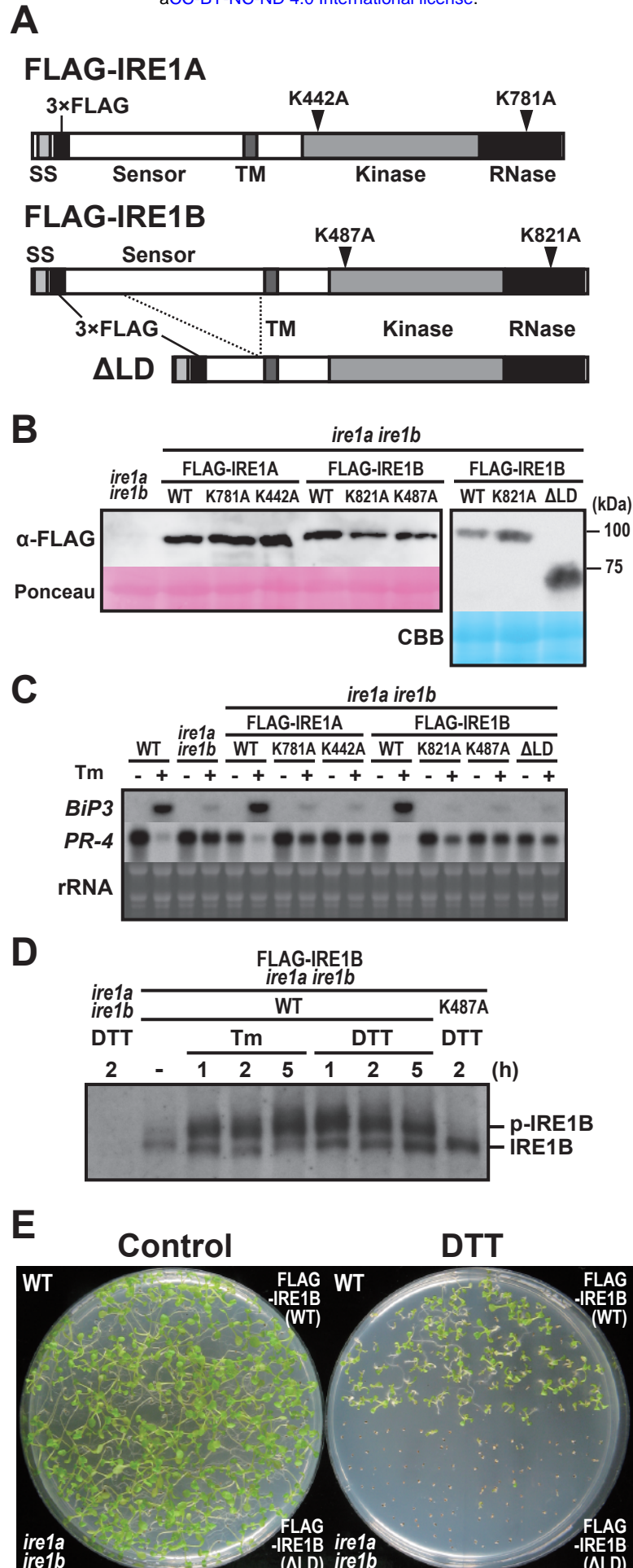


Figure 3

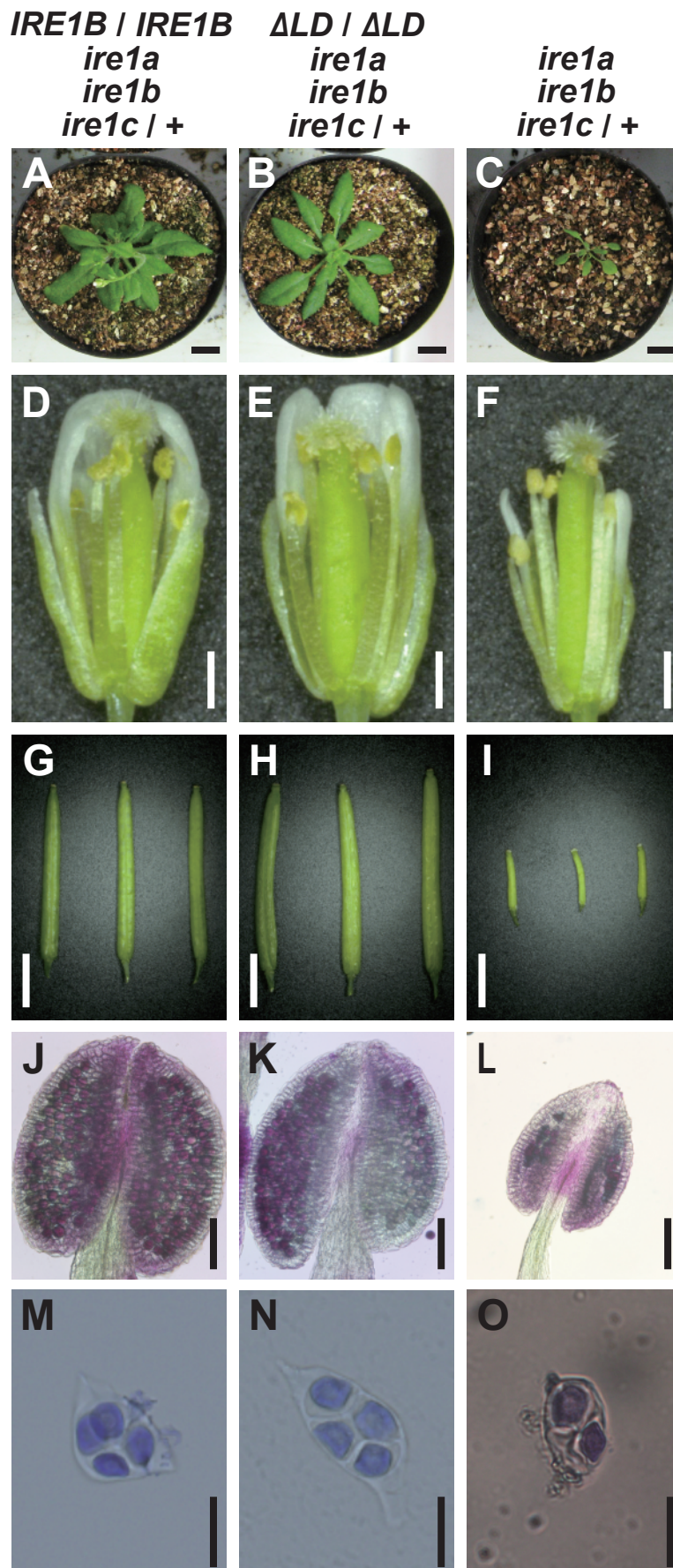


Figure 4

WT

***ire1a*
ire1b
ire1c / +**

**ΔLD / ΔLD
ire1a
ire1b
ire1c / +**

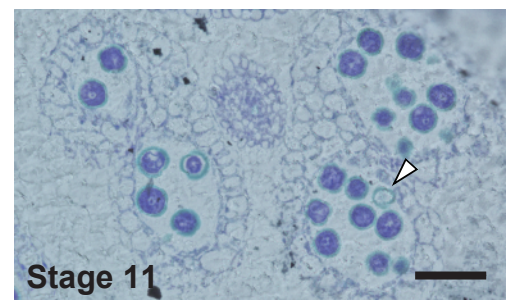
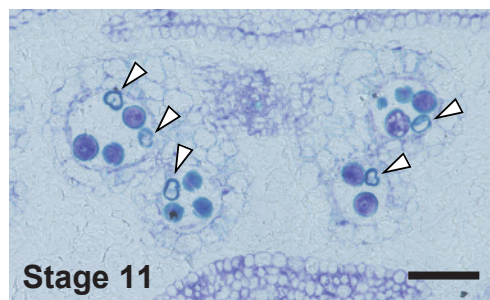
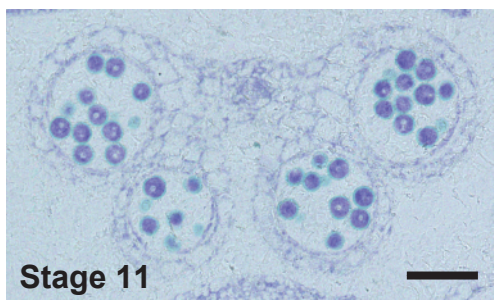
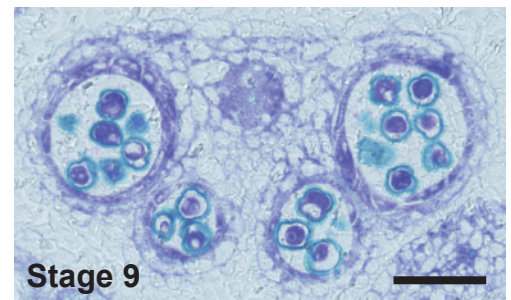
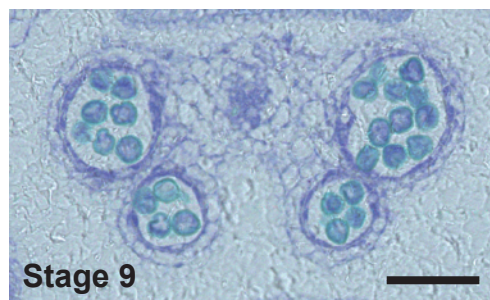
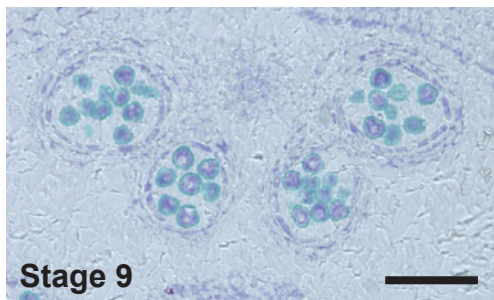
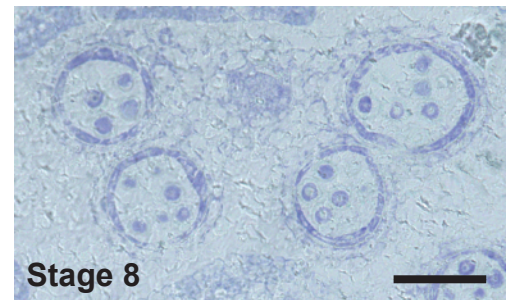
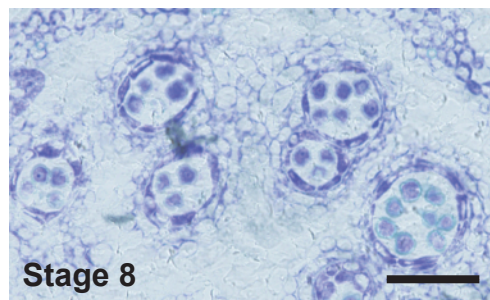
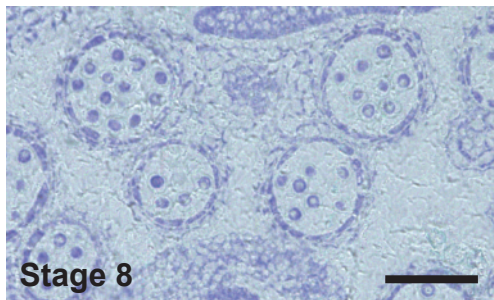


Figure 5

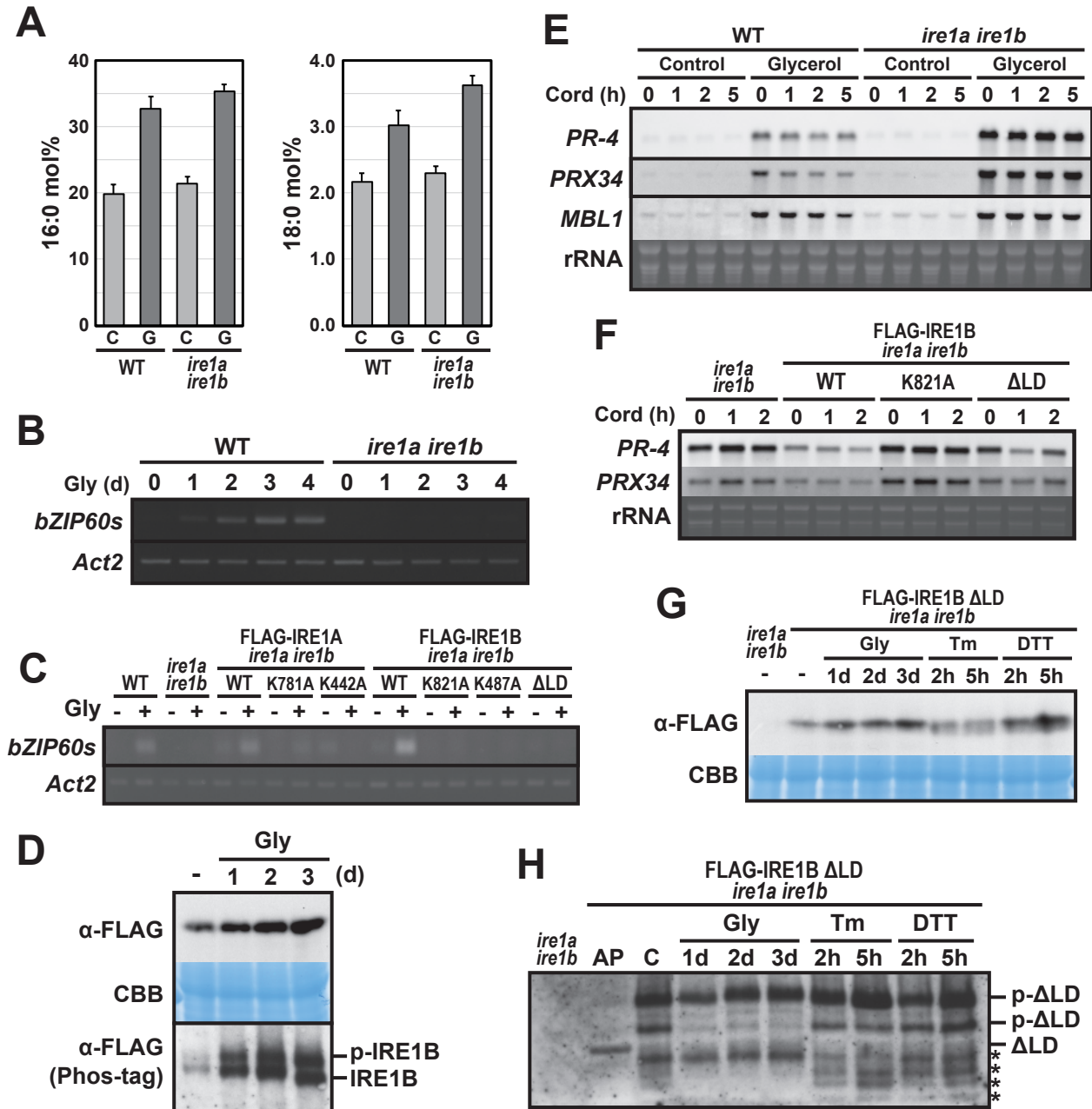


Figure 6

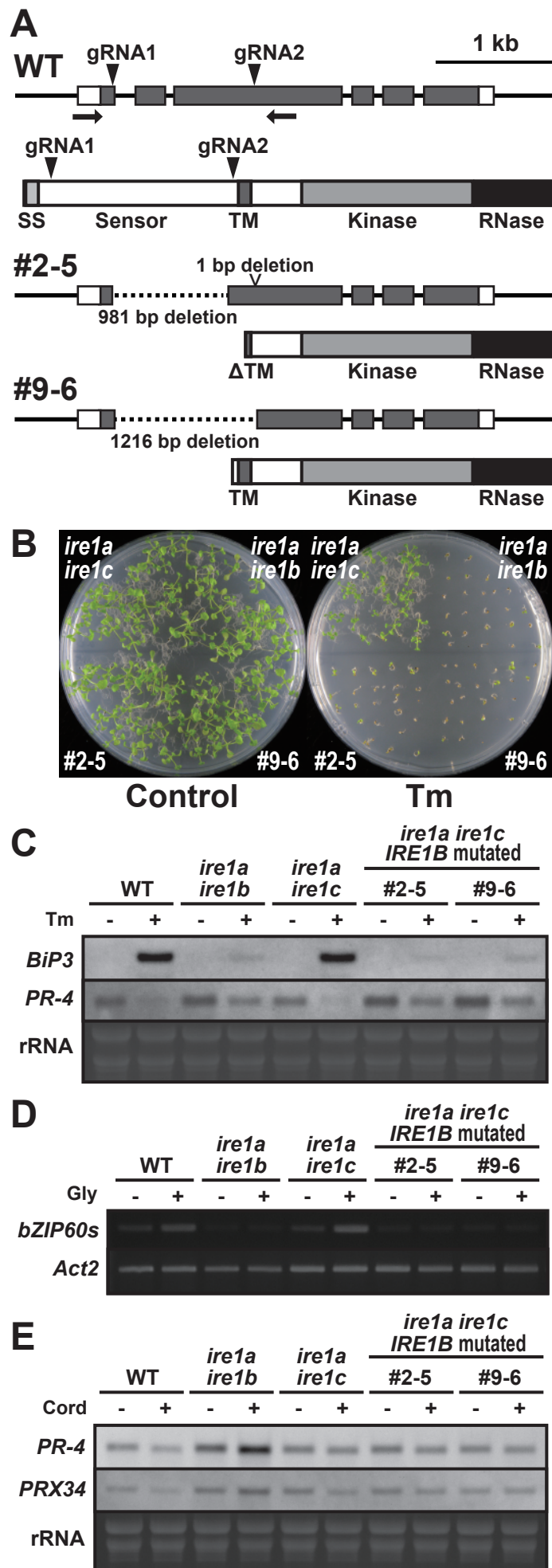


Figure 7